5th International Symposium on Three-Dimensional Electromagnetics
Sapporo, Japan, May 7-9, 2013

# Three-dimensional simulation of the electromagnetic fields induced by tsunamis: A case study for the 2011 Tohoku Tsunami

Luolei Zhang, Hisashi Utada, Hisayoshi Shimizu, Kiyoshi Baba, Takuto Maeda
Earthquake Research Institute, University of Tokyo, Tokyo, Japan

## SUMMARY

The motion of seawater induces electromotive force of significant intensity due to Faraday's law, and resulting electromagnetic field can be recorded by instruments installed on land or at ocean bottom. However, a few studies were successfully simulating motionally induced electric and magnetic fields by an exact and accurate application of Maxwell equations. We built an accurate scheme for numerical simulation to calculate EM fields due to ocean tidal flow, and tested the accuracy by using the source currents in the ocean as expected from a Tohoku Tsunami simulation. The source current distribution is predicted by the flow data calculated by a tsunami simulation in 2-D Cartesian coordinates based on the linear long-wave theory. From the calculated source currents, the three components of magnetic variations were estimated by the forward code. We compared the calculated magnetic field with that observed in response to the devastating Tohoku tsunami of 2011 not only on land observatories but also at some seafloor sites, to check the accuracy of the code. It shows that our results are in good agreement with observations. We also get some characteristics of different components of magnetic field on the seafloor.

**Keywords**: 3-D forward calculation, tsunami, magnetic field, earthquake

## INTRODUCTION

The motion of seawater induces electromotive force of significant intensity (Sanford, 1971) due to Faraday's law, and resulting electromagnetic (EM) field can be recorded by instruments installed on land or at ocean bottom (Tyler, 2005; Toh et al., 2011). However, only a few studies were successfully simulating tsunami induced EM fields by an exact and accurate application of Maxwell equations that is essential for a quantitative interpretation to get geophysical information from observations of related EM signals. Here we present a 3-D modeling scheme to simulate these observed fields. We apply a 3-D EM induction integral equation code in Cartesian coordinate system with a heterogeneous source term, which is based on the modified iterative dissipative method (MIDM) (Singer 1995; Zhang et al. 2012).

## SIMULATION METHOD

### Induction Equation

For electromagnetic field time variations, assuming a harmonic time dependence of $e^{-i\omega t}$ where $i = \sqrt{(-1)}$ and $\omega$ is the angular frequency, Maxwell equations can be written as

$$\frac{1}{\mu_0}\nabla\times\mathbf{B}(\mathbf{r};\omega)=\sigma(\mathbf{r})\mathbf{E}(\mathbf{r};\omega)+\mathbf{J}^{ext}(\mathbf{r};\omega)$$
$$\nabla\times\mathbf{E}(\mathbf{r};\omega)=i\omega\mathbf{B}(\mathbf{r};\omega) \quad (1)$$

In these equations, **E** and **B** are the electric and magnetic fields, $\sigma$ and $\mu_0$ denote the electrical conductivity and magnetic permeability of free space, and $\mathbf{J}^{ext}$ is the extrinsic (source) current.

For a moving conductor such as sea water flow, the equations also can be used, but the extrinsic current $J^{ext}$ is calculated as

$$\mathbf{J}^{ext}(\mathbf{r},\omega)=\sigma_w(\mathbf{r})\cdot(\mathbf{v}(\mathbf{r},\omega)\times\mathbf{B}_0(\mathbf{r})) \quad (2)$$

where $\sigma_w$ is the electrical conductivity of the moving conductor, here is the sea water conductivity, which equals 3.2 S/m, **v** is the vector of the fluid velocity, $\mathbf{B}_0$ is the vector of the main magnetic field derived from a model IGRF at each point. The time variation in $\mathbf{B}_0$ is small so that $\mathbf{B}_0$ is assumed to be time independent.

### Theory of Integral Equation Method

The Earth is assumed to be a half space, with a 3-D heterogeneous conductivity distribution $\sigma(\mathbf{r})$ consisting of a reference medium having a 1-D distribution and a lateral perturbation, so that $\sigma(\mathbf{r}) = \sigma_0(z) + \Delta\sigma(\mathbf{r})$. Considering the linearity of Maxwell equations with respect to the electric and magnetic fields, they are assumed to be composed of the primary fields due to the reference medium and the secondary fields due to scattering by the heterogeneity, i.e., $\mathbf{E} = \mathbf{E}_p + \mathbf{E}_s$ and $\mathbf{B} = \mathbf{B}_p + \mathbf{B}_s$. Here, the primary fields $\mathbf{E}_P$ and $\mathbf{B}_p$ are excited by the externally imposed current $\mathbf{J}^{ext}$ in the reference distribution of conductivity $\sigma_0$ and can be expressed as

$$\mathbf{E}_p(\mathbf{r};\omega)=\int_v \mathbf{G}_0^E(\mathbf{r},\mathbf{r}';\sigma_0;\omega)\cdot\mathbf{J}^{ext}(\mathbf{r}';\omega)dv'$$
$$\mathbf{B}_p(\mathbf{r};\omega)=\mu_0\int_v \mathbf{G}_0^H(\mathbf{r},\mathbf{r}';\sigma_0;\omega)\cdot\mathbf{J}^{ext}(\mathbf{r}';\omega)dv' \quad (3)$$

where $\mathbf{G}_0{}^E$ and $\mathbf{G}_0{}^H$ are the electric and magnetic dyadic Green's tensors for Maxwell equations in a reference medium, $v$ denotes the space where the external current

distributes, **r** and **r'** denote the locations of observation site and of discretized heterogeneity, and $z$ is the vertical coordinate. Since $\mathbf{E}_p$ and $\mathbf{B}_p$ both satisfy Equation (1) in a reference medium, scattered fields satisfy Maxwell equations, which can be written as follows:

$$\frac{1}{\mu_0}\nabla\times\mathbf{B}_s(\mathbf{r};\omega)=\sigma_0(z)\mathbf{E}_s(\mathbf{r};\omega)+\mathbf{J}^q(\mathbf{r};\omega)$$
$$\nabla\times\mathbf{E}_s(\mathbf{r};\omega)=\mathrm{i}\omega\mathbf{B}_s(\mathbf{r};\omega) \quad (4)$$

where

$$\mathbf{J}^q(\mathbf{r};\omega)=(\sigma(\mathbf{r})-\sigma_0(z))\mathbf{E}(\mathbf{r};\omega)$$
$$=\mathbf{J}^s(\mathbf{r};\omega)+(\sigma(\mathbf{r})-\sigma_0(z))\mathbf{E}_s(\mathbf{r};\omega) \quad (5)$$

and

$$\mathbf{J}^s(\mathbf{r};\omega)=(\sigma(\mathbf{r})-\sigma_0(z))\mathbf{E}_p(\mathbf{r};\omega) \quad (6)$$

where $\sigma_0$ is the conductivity of 1-D medium, $\sigma$ is the conductivity of 3-D medium. Then the solution for secondary field can be expressed,

$$\mathbf{E}_s(\mathbf{r};\omega)=\int_{v_{3D}}\mathbf{G}_0^E(\mathbf{r},\mathbf{r}';\sigma_0;\omega)\cdot\mathbf{J}^q(\mathbf{r}';\omega)dv'$$
$$\mathbf{B}_s(\mathbf{r};\omega)=\mu_0\int_{v_{3D}}\mathbf{G}_0^H(\mathbf{r},\mathbf{r}';\sigma_0;\omega)\cdot\mathbf{J}^q(\mathbf{r}';\omega)dv' \quad (7)$$

The integral equation (7) is solved by the MIDM (Singer 1995; Zhang et al. 2012).

### Model Construction and Source Current Calculation

For the model construction, we refer to the 1-D model (Baba et al., 2010) for the Northwest Pacific and Philippine Sea. We also have the accurate topographic map of the seafloor. Above the seafloor, we assume the sea water conductivity to be constant. Under the seafloor, a 1-D structure is assumed at each grid point. Thus, for this case study, we can get a simple 3-D electrical conductivity structure with only lateral heterogeneity due to undulating seafloor topography (Figure 1). However, it is possible to assume a more complex 3-D distribution of sub-seafloor conductivity, if such a situation is interested.

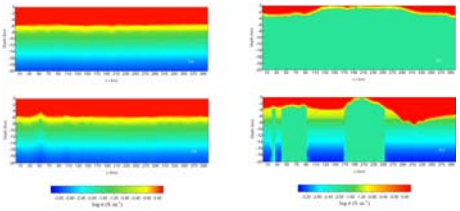


**Figure 1.** N-S (top) and E-W (bottom) cross sections of the conductivity structure model for CBI (left) and NM04 (right) based on Baba et al. (2010).

The source current distribution is predicted by the flow data calculated by a tsunami simulation in 2-D Cartesian coordinates based on the linear long-wave theory (Maeda and Furumura, 2011). Velocity data from tsunami simulation for 180 minutes after the origin time of the Tohoku earthquake were transformed to the frequency domain at each grid point for the MIDM solver. The frequency domain solutions of Maxwell equations are then transformed back to the time domain to be compared with observations. Comparisons in the frequency domain are also possible.

### Area Size and Grid Spacing

We simulated the electromagnetic fields observed at Chichijima island (CBI) and at a seafloor site in the northwest Pacific (NM04) (Figure 2). First we tested several EM simulations with different area size, including 200 km×200 km, 400 km×400 km, 800 km×800 km and 1200 km×1200 km, by using the same horizontal grid spacing. From the comparison of results, we concluded that 800 km×800 km is optimum for CBI and 400 km × 400 km is optimum for NM04 by considering the computation accuracy and cost.

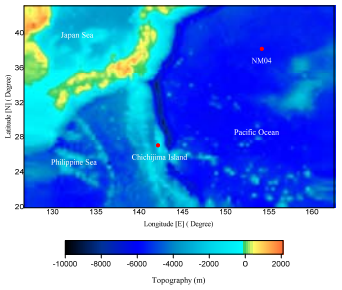


**Figure 2.** Positions of observation points (CBI and NM04)

We also tested several simulations with different grid spacing, such as 100 m, 1 km, 2 km, and 4 km, by using the same area size. From comparison, we concluded 1km grid spacing is small enough to accurately evaluate electro-magnetic field.

### Convergence

Convergence of the integral equation (7) was confirmed by a criterion that the normalized residual becomes $O(10^{-8})$ for each frequency. To attain convergence, about 20 iterations are performed.

## SIMULATION RESULTS

### CBI (island site)

Figure 3 shows results for CBI. In Figure 3a, the vertical component calculated using Biot-Savart law (e.g. Utada et al., 2011) and that of the primary field from 3-D simulation were compared with observations. We can see the qualitative agreement in arrival time but model results are greater in amplitude than observation. However the result from the 3-D simulation show amplitude slightly smaller than observation (Figure 3b). There is also a small time shift between simulation result and observation. We consider these discrepancies are

caused by the inaccuracy of the tsunami simulation in the Cartesian coordinate system (sphericity of Earth is significant). Lateral heterogeneities would convert the toroidal to poloidal mode but the amplitude of converted mode is generally much smaller than that of original poloidal mode. Therefore the source of the toroidal mode can be ignored in case of modeling observations on land.

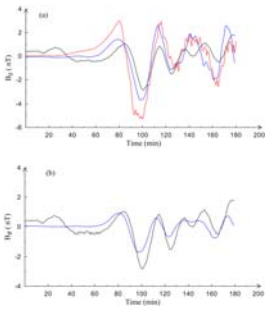

**Figure 3.** Simulated $B_z$ at Chichijiama Island: (a) $B_z$ using Biot-Savart law (red line) and primary field of 3-D calculation (blue line) and observation (black line); (b) simulation result (blue line) and observation (black line)

**NM04 (seafloor site)**

Results for a seafloor site NM04 are shown in Figures 4a-4d, in which we notice a reasonable agreement between models and observations.

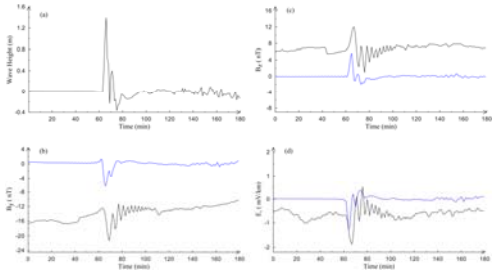

**Figure 4.** Simulation results (blue lines) and observations (black lines) at NM04: (a)Wave height; (b) Horizontal magnetic field $B_y$; (c)Vertical magnetic field $B_z$; (d) Horizontal electrical field $E_x$

Here we examine how the toroidal source can be effective for modeling seafloor observations. Figure 5 is the comparison between vertical vorticity and horizontal divergence of the velocity, which control the efficiency of the toroidal and poloidal mode generations, respectively. We can see the vorticity can be about 1/3-1/2 of the divergence when seabed is very conductive. The toroidal mode should be taken into account for modeling seafloor observations, especially the horizontal magnetic field perpendicular to the dominant tsunami propagation direction.

We also examined how the tsunami-induced EM field observations constrain the conductivity of the shallower part of the seabed, which is difficult to be resolved by using ordinary seafloor magnetotelluric signals. We found the toroidal mode is sensitive to the integrated resistivity of sediment layer (1km thick) (Figure 6), while the poloidal mode is mostly sensitive to the integrated conductivity of the deeper structure (deeper than 30 km in this case). (Figure 7)

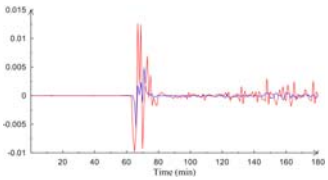

**Figure 5.** The comparison between vertical vorticity (blue line) and horizontal divergence (red line) of the velocity.

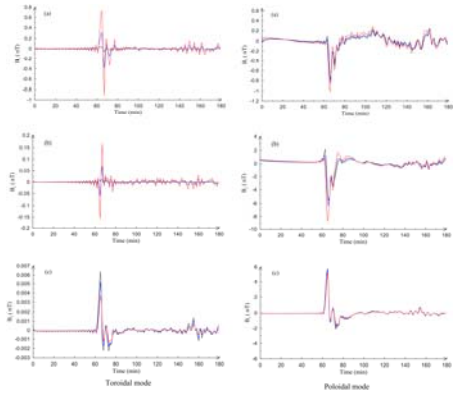

**Figure 6.** Effect of the conductivity of the sediment on the induced magnetic field at NM04. Black, blue, red lines show the case with 0.1,1 and 3S/m, respectively

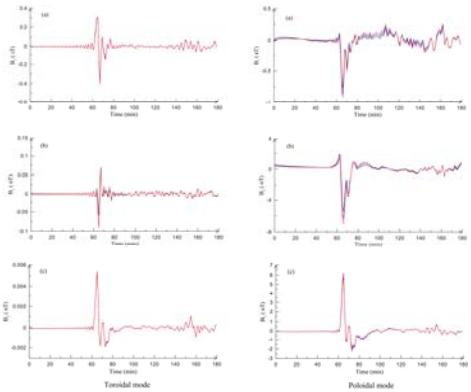

**Figure 7.** Effect of the conductivity of the deeper part on the induced magnetic field at NM04. Assumed conductivity was $\sigma_0$(black), $100\sigma_0$ (blue), $500\sigma_0$ (red), where $\sigma_0$ is the background 1-D conductivity

**Motional magnetotellurics**

If a tsunami passes a seafloor MT observation, we have simultaneous record of electromagnetic field. Then a treatment of EM field data similar to the magnetotelluric processing can be applied.
We also define the impendence and tipper as:

$$Z_{tr}(\mathbf{r};\omega)=\frac{E_t(\mathbf{r};\omega)}{B_r(\mathbf{r};\omega)}, M_{zr}(\mathbf{r};\omega)=\frac{B_z(\mathbf{r};\omega)}{B_r(\mathbf{r};\omega)} \quad (8)$$

where suffixes t , r and z stand for the transverse, radial and vertical directions relative to the tsunami propagation direction. For a 1-D long wave propagating in y direction, they can be related as,

$$Z_{tr}(\mathbf{r};\omega)=\frac{\omega}{k}M_{zr}(\mathbf{r};\omega) \quad (9)$$

where k is the wave number (Shimizu et al., 2013, in prep.). We calculate the amplitude and phase of $Z_{xy}$ and $M_{zy}$•k/ω from the observations (Figure 8) and simulation results (Figure 9). We compared the amplitude and phase of calculated impendence and tipper with those calculated by half spaces with uniform resistivity of 1 Ω-m (blue line), 10 Ω-m (green line) and 100 Ω-m (red line). We notice that the motional impedance and tipper can be an easy indicator for exploring the crust and mantle but useful only at longer periods. When the period is shorter, the response functions only indicate the mean ocean depth, because the impedance amplitude approaches to the phase velocity of the long wave. All curves of $Z_{xy}$ and $M_{zy}$•k/ω (black line) from simulations and observations are rather in good agreement, which means the sea bed structure is close to 1-D.

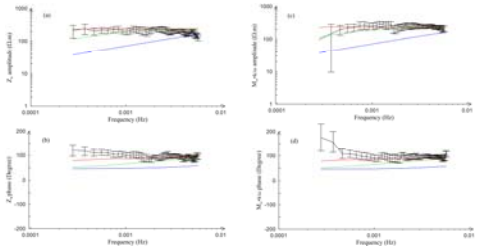

**Figure 8.** Motional impedance and tipper : observations at NM04 and 1-D half space (0.01, 0.1, 1 S/m)

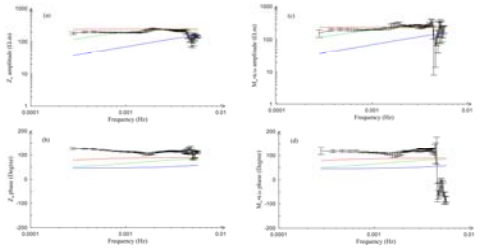

**Figure 9.** Motional impedance and tipper : 3-D simulation results at NM04 and 1-D half space (0.01, 0.1, 1 S/m)

## CONCLUSIONS

Measured fields on the island (and land) are mostly due to the poloidal sources. At the seafloor, poloidal mode due to horizontal motion is still dominant. The contribution of each toroidal mode may not be negligible if the seabed is very conducting. Poloidal mode is sensitive mostly to the conductivity of deep structure (down from 30 km). Toroidal mode may not be negligible, and is sensitive to the integrated resistance of the sediment layer (about 1km thick). Motional impedance and tipper can be an easy indicator for exploring the crust and mantle but useful only at longer periods. For shorter period, these response functions only indicate the mean ocean depth (the phase velocity of long wave).

## REFERENCE


Baba, K., Utada, H., Goto, T., et al., 2010. Electrical conductivity imaging of the Philippine Sea upper mantle using seafloor magnetotelluric data. *Phys. Earth Planet. Int.*, **183**, 44-62.

Kuvshinov, A., Junge, A., Utada, H., 2006. 3-D modelling the electric field due to ocean tidal flow and comparison with observations. *Geophys. Res. Lett.*, **33**, 6314, doi:10.1029/2005GL025043.

Maeda, T., Furumura, T., Sakai, S., et al., 2011. Significant tsunami observed at ocean-bottom pressure gauges during the 2011 off the Pacific coast of Tohoku Earthquake. *Earth Planets Space*, **63**, 803–808.

Sanford, T. B., 1971. Motionally induced electric and magnetic fields in the sea. *J. Geophys. Res.*, **76**, 3476–3492.

Singer, B. Sh., 1995. Method for solution of Maxwell's equations in non-uniform media. *Geophys. J. Int.*, **120**, 590-598.

Toh, H, Satake, K., Hamano, Y., Fujii, Y., Goto, T., 2011.Tsunami signals from the 2006 and 2007 Kuril earthquakes detected at a seafloor geomagnetic observatory, *J. Geophys. Res.*, **116**, B02104, doi:10.1029/2010JB007873.

Tyler, 2005. A simple formula for estimating the magnetic fields generated by tsunami flow. *Geophys. Res. Lett.*, **32**, L09608, doi:10.1029/2005GL022429.

Utada, H., Shimizu, H., Ogawa, T., Maeda, et al., 2011. Geomagnetic field changes in response to the 2011 off the Pacific Coast of Tohoku Earthquake and Tsunami. *Earth Planet. Sci. Lett.*, **311**, 11-27.

Zhang, L., Koyama, T., Utada, H., et al., 2012. A regularized three-dimensional magnetotelluric inversion with a minimum gradient constrain. *Geophys. J. Int.*, **189**, 296-316.